IDETC2016-60171

A MEMS MICROPHONE USING REPULSIVE FORCE SENSORS

Mehmet Ozdogan
Department of Mechanical Engineering
Binghamton University
Binghamton, New York 13902
Turkish Military Academy
Ankara, Turkey 06654
Email: mozdoga1@binghamton.edu

Shahrzad Towfighian *
Dept. of Mechanical Engineering
Binghamton University
Binghamton, New York 13902
Email: stowfigh@binghamton.edu

ABSTRACT

We present a MEMS microphone that converts the mechanical motion of a diaphragm, generated by acoustic waves, to an electrical output voltage by capacitive fingers. The sensitivity of a microphone is one of the most important properties of its design. The sensitivity is proportional to the applied bias voltage. However, it is limited by the pull-in voltage, which causes the parallel plates to collapse and prevents the device from functioning properly. The presented MEMS microphone is biased by repulsive force instead of attractive force to avoid pull-in instability. A unit module of the repulsive force sensor consists of a grounded moving finger directly above a grounded fixed finger placed between two horizontally seperated voltage fixed fingers. The moving finger experiences an asymmetric electrostatic field that generates repulsive force that pushes it away from the substrate. Because of the repulsive nature of the force, the applied voltage can be increased for better sensitivity without the risk of pull-in failure. To date, the repulsive force has been used to engage a MEMS actuator such as a micro-mirror, but we now apply it for a capacitive sensor. Using the repulsive force can revolutionize capacitive sensors in many applications because they will achieve better sensitivity. Our simulations show that the repulsive force allows us to improve the sensitivity by increasing the bias voltage. The applied voltage and the back volume of a standard microphone have stiffening effects that significantly reduce its sensitivity. We find that proper design of the back volume and capacitive fingers yield promising results without pull-in instability.

INTRODUCTION

A MEMS microphone is a type of acoustic sensor that transduces acoustic signals into electrical output. MEMS microphones are widely used in many applications such as hearing aids [1,2], sound localizations [3], surveillance systems [4], consumer electronics (e.g. smart phones and tablets) and speech recognition systems [5]. Among different sensing mechanisms, capacitive sensors are the most common in MEMS microphones because of their high stability, sensitivity and signal to noise ratio [6–11]. A capacitive based microphone consists of two parallel electrodes (a diaphragm and a back plate) that produces output voltage from the movement of the electrically loaded diaphragm in response to sound pressure variation on its surface area.

Microphones may be classified by their sensitivity, noise performance, frequency bandwidth, dynamic range and directivity (directional or non-directional) [12]. The sensitivity of the capacitive microphone is proportional to the applied bias voltage and the surface area of the diaphragm and is inversely proportional to stiffness of the springs [6, 7]. Hence, to improve the sensitivity, it is necessary to increase the surface area of the diaphragm and bias voltage or to reduce mechanical stiffness. Increasing the size of the microphone is against the miniaturization trend and decreasing the mechanical stiffness has limited poten-

---

*Address all correspondence to this author.

tial. The alternative way to increase the sensitivity of the microphones is to increase the bias voltage; however, that is severely limited by the pull-in voltage of the parallel-plate electrodes. To address this challenge, we investigated a MEMS microphone that uses repulsive force fingers to detect the variation of mechanical movement of a diaphragm caused by the sound pressure.

The concept of repulsive force was introduced for large stroke electrostatic actuation by He et al. [13]. The main purpose of our study is to investigate the application of this concept for a capacitive MEMS microphone. By properly designing of the microphone, one can generate a repulsive force on the moving fingers, pushing the diaphragm away from the substrate. This property eliminates the undesired pull-in effect and allows increasing the bias voltage to achieve higher sensitivity.

The structure of the paper is as follows: First, we give some background for MEMS microphones and the relation between design parameters and sensitivity. In this part, we also review some alternative methods to avoid pull-in instability. Second, we describe the model and governing mathematical equations. Then, we investigate the effect of air slits and back volume on the response of the diaphragm. Last, we discuss simulation results and give a conclusion.

MICROPHONE BACKGROUND

Advancing MEMS fabrication technology encouraged researchers to develop new silicon microphones after their first fabrication by Royer et al. [14]. Most conventional microphones consist of a rotating or a translating diaphragm and a back plate. As a sound pressure wave reaches the diaphragms surface, it deflects. This deflection produces an electrical output. Almost all microphone types such as piezoelectric, piezoresistive, optical and capacitive microphone work on this principle.

Piezoelectric and Piezoresistive Microphones

Piezoelectric microphones use the piezoelectric effect to produce an electric output from the diaphragm deflection [15]. Piezoelectric ceramics can perform up to very high frequency ranges, which is advantageous for microphone performance [12]. Some applications include aircraft noise detection [16], or audio-range sensing [17]. William et al. [16] reported the sensitivity as 39 μV/Pa. Frequency bandwith was up to 20 kHz and the resonance frequency was 129.5 kHz. The microphone by Baumgartel et al. [17] had greater than 2.5 mV/Pa unamplified sensitivity between 0.24 kHz-6.5 kHz.

Piezoresistive microphones use the piezoresistive effect of silicon to obtain an electrical output. Stress sensitive material is doped on the membrane. A stress in the membrane creates a change in the resistance that corresponds to electric current by the piezoresistive mechanism. The sensitivity of these type of microphones can be increased by having larger bias voltage.

However, induced current increases temperature and causes thermal noise. In addition to high thermal noise these microphones have poor dynamic range [12] and low sensitivity compared to other types [15].

In 2014, Zhou et al. [18] presented a piezoresistive aero-acoustic microphone with the sensitivity of 0.33 μV/V/Pa and high frequency bandwidth of 520 kHz. The authors investigated the mechanical response of the device with different damping designs for the squeeze film damping effect. They also mention that significant amount of strong mechanical resonance is attenuated with their design.

Optical Microphone

Optical microphones were introduced for accurate acoustic measurements in harsh environments that experience a wide temperature range. Using integrated light modulators, light signals are converted into electric outputs by optical microphones [19, 20]. The optical microphones were presented as an alternative method to avoid pull-in [21, 22]. The challenge with optical microphones is the need for an external stable reference light that does not affect the sensitivity of the device because the sensitivity is independent of diaphragm area and is related to the reference light source.

Capacitive Microphones

Like other types of microphones, capacitive microphones have movable, thin diaphragms and back plates. The capacitive transduction mechanism is the most common type used because of its high stability, sensitivity and signal to noise ratio. However, the microphones suffer from pull-in instability, which causes the diaphragm and back plate to stick to each other above a certain voltage because of the electrostatic attractive force between the plates. To overcome this instability, researchers developed different designs for capacitive microphones such as dual back plates [23, 24].

During the years, capacitive microphones have evolved a great extent. Developing MEMS fabrication technology encourages researchers to have the opportunity for improving and minimizing the silicon microphones after its first fabrication by Royer et al. [14]. In 1984, a capacitive MEMS microphone was reported by Hohm et. al [25]. The device had the resonance frequency of 8.5 kHz. The sensitivity was reported as 3 mV/Pa at the operation voltage of 350 V and frequency of 1 kHz. The measured capacitance was around 9 pF. In 1994, Berqvist et al. [26] presented the first electroplated capacitive microphone. For 28 V of applied bias voltage, the sensitivity was measured as 1.4 mV/Pa. The dynamic range was limited by the resonance frequency of around 14 kHz for this device with the total capacitance of 5.4 pF. In 2002, Rombach et al. [23] presented the first low-noise, low-voltage, directional, dual back plate microphone. At 1 kHz and 1.5 V bias voltage, the sensitivity was reported as

13 mV/Pa. In 2014, Miles et al. [27] presented a MEMS low-noise, pressure-gradient, directional microphone by using inter-digitated comb fingers. They reported high sensitivity to sound pressure gradients.
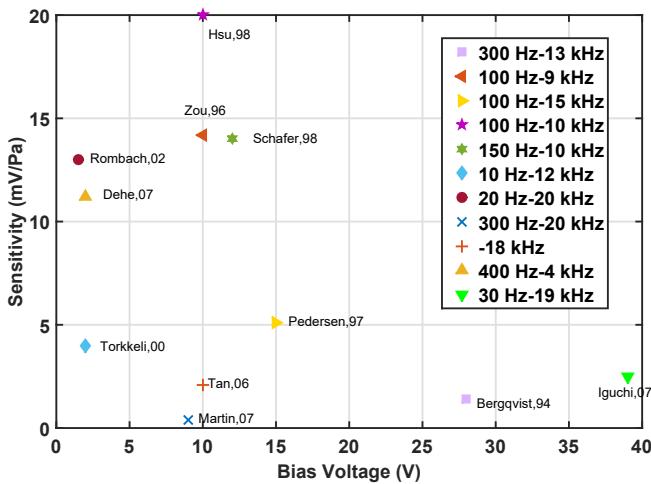

FIGURE 1: Sensitivity and bandwidth comparison of some selected capacitive microphones from literature.

Sensitivity

In MEMS capacitive sensor design, sensitivity is one of the most important factors as well as stability and dynamic range. The sensitivity is the ratio of the output change over the input change. It has two parts: mechanical and electrical sensitivity. Mechanical sensitivity is the increase in the deflection of the moving plate as the pressure increases. Electrical sensitivity is the capacitance change as the deflection increases. These sensitivities can be represented as

$$S_{mc} = \frac{\Delta y}{\Delta P} \quad \text{or} \quad S_{mc} = \frac{\Delta \theta}{\Delta P} \tag{1}$$

$$S_{ec} = \frac{\Delta C}{\Delta y} \quad \text{or} \quad S_{ec} = \frac{\Delta C}{\Delta \theta} \tag{2}$$

where Δy, $\Delta \theta$, ΔP and ΔC are the changes of position of the moving plate (deflection), rotation angle, pressure and capacitance, respectively.

The effect of key design parameters of a non-directional capacitive microphone on the overall sensitivity is estimated by

TABLE 1: Effect of Parameters on a Conventional Microphone Specifications (Sen.:Sensitivity, Cap.:Capacitance-, Vp:Pull-in voltage ↑:Increase, ↓:Decrease, ↔:unaffected)

Parameter	Case	Sen.	Cap.	Noise	Vp
Diaphragm Area (A)	↑	↑	↑	↓	↓
Bias Voltage (V_{bias})	↑	↑	↑	↔	↔
Air Gap (d)	↑	↓	↓	↓	↑
Stiffness (K)	↑	↓	↔	↑	↑

$S = AV_{bias}/(Kd)$ [6], where A is the diaphragm area, d is the air gap between diaphragm and backplate, K is the spring stiffness or effective stiffness of the device and V_{bias} is the applied bias voltage. For parallel plat electrodes, the bias voltage is limited to the pull-in voltage calculated by $V_p = \sqrt{(8/27) \cdot (Kd^3/(\varepsilon A)}$ where ε is air permittivity. Table 1 provides a summary of the effect of microphone design parameters on sensitivity, capacitance, noise, and pull-in voltage. To create a high performance microphone, all of these parameters should be designed together. In this study, we present a MEMS microphone using repulsive force sensors that avoid pull-in instability to achieve high sensitivity.

MODEL DESCRIPTION AND OPERATION PRINCIPLE
Electrostatic Actuation and Repulsive Force

Micro-devices employing electrostatic force are widely preferred in the MEMS area because of their low fabrication cost, small size, and ease of integration into various systems [28]. The electrostatically actuated devices have been designed with different configurations of parallel plate actuators. In this type of actuation, there are two electrodes: one is moving and the other is fixed. The moving electrode deflects towards to the fixed one when a specific electrostatic load is applied. The deflection occurs from the electrostatic force generated by an electric field between these charged plates [29]. However, as the applied electrostatic load goes beyond a certain limit, it causes a dramatic collapse of the upper plate, which sticks to the fixed one by the attractive force. The main reason of this collapse is the restoring force that can no longer overcome the electrostatic attractive force. This phenomenon is called as pull-in instability and to avoid it, many presented studies have used techniques such as comb-drive fingers, fringing-field based configurations [30–33] and repulsive force (out-of plane) designs [13, 34].

MEMS devices that use comb-drive actuators may avoid pull-in, but they suffer from low travel ranges. To extend their stroke they are actuated around their resonance frequencies

[30].As an alternative to comb-finger actuators, fringing electro-static field type actuators were presented by Lee et al. [30]. In this type of actuation mechanism there are basically two station-ary electrodes and one moving plate or beam. In this method, an electrostatic load is applied to stationary electrodes and the moving plate is grounded. A generated electrostatic field in-duces the electrostatic force to displace the moving plate. The repulsive force is another method to overcome pull-in instabili-ties [13]. The force is induced by the asymmetric electrostatic field of the moving and fixed fingers. A MEMS actuator using repulsive force is a widely studied subject in literature [35–38]. However, it has been used for only actuation mechanisms. In 2015, Zhou et al. [39] proposed that this method is also a promis-ing alternative to avoid pull-in instabilities for capacitive sensing mechanisms. In this paper we will investigate the application of the electrostatic repulsive force for a microphone design.

Repulsive Sensor Unit Cell Design

The unit cell of the repulsive sensor is composed of mov-ing fingers attached to a diaphragm, voltage fixed fingers and grounded fixed fingers, Figure (2). This configuration was in-troduced by He et al. [13, 35] to produce a repulsive force (out-of-plane) on the moving finger for actuation. In a prior study, the authors presented the feasibility of using the repulsive force concept as a sensing mechanism for micro devices [39]. In a unit cell of the sensor, a net repulsive force is generated on the moving finger by the electrostatic attractive forces of the fixed electrodes on both sides of the moving finger. The role of the grounded fixed finger is to break the symmetry in the electrostatic field of the moving finger so the forces on its top surface become larger than its bottom surface, creating a net repulsive force that pushes the moving finger away from the substrate. The microphone de-sign using the repulsive force sensor is depicted in Figure (3) with the parameters listed in table 2. The material is assumed to be polysilicon. The diaphragm is suspended using two short cantilever beams fixed on the substrate. The repulsive force act-ing on the moving fingers will result in the rotational motion of the diaphragm around the rotation axis. The stiffness and mass moment of inertia of the model were obtained from finite ele-ment package of ANSYS. Three modes of the vibration of the diaphragm are presented in Figure (4).

There are a number of fingers attached to three sides of the diaphragm. We simulate various scenarios to obtain maximum electrostatic force. FEM Simulations are done for four differ-ent cases: Case 1) We choose the thickness and width of all the fingers as 2 microns and 3 microns, respectively. Case 2) the thickness and width of all the fingers are chosen as 2 microns and 4 microns, respectively. Case 3) The thickness and width are selected as 2 microns and 5 microns, respectively. Case 4) For the last scenario, to increase the electrostatic force, the width of all the fingers and the thickness of the voltage fixed finger are 4

microns, but the thickness of other fingers are 2 microns. The electric field distribution for the unit cell of the last scenario is depicted in Figure (2).
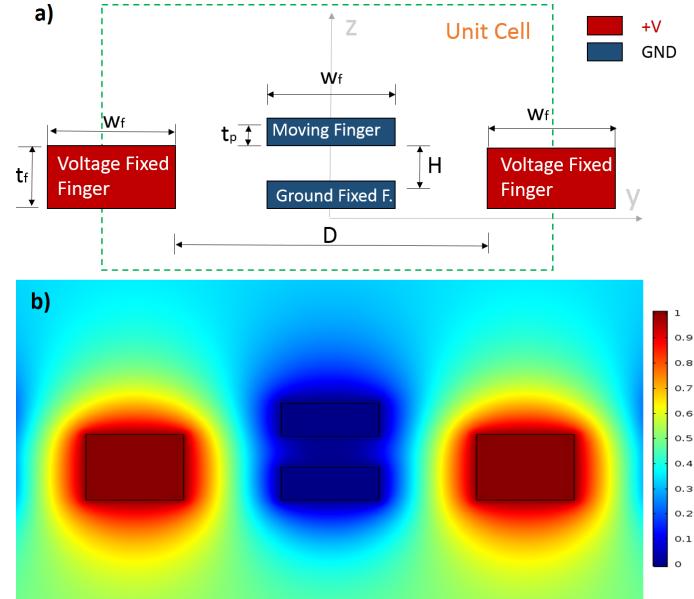

FIGURE 2: a) Unit cell of repulsive force sensor. b) The electro-static field around the moving and fixed fingers when the applied Voltage is 1 Volt (Case 4).

MATHEMATICAL MODEL

For a simplified lumped-parameter model of the diaphragm, the governing equation for rotational motion is given by [27]

$$I\ddot{\theta} + K_t\theta + C_t\dot{\theta} = T(t) + \frac{V^2}{2}\frac{dC}{d\theta} \tag{3}$$

where I is the mass moment of inertia of the diaphragm about the y axis. K_t is the stiffness of the structure, C_t is the torsional damping constant, T is the applied moment by the sound pres-sure. C is the capacitance that is found from the finite element package of COMSOL.

Estimating Capacitance using finite element method

To find the total capacitance of the model, we first find the capacitance for a unit cell of the repulsive sensor (Figure (2)) using COMSOL and then integrate it across the moving finger length to find the total capacitance of the device used in the Equa-tion (3). The unit cell capacitance is a function of the vertical

Copyright © 2016 by ASME
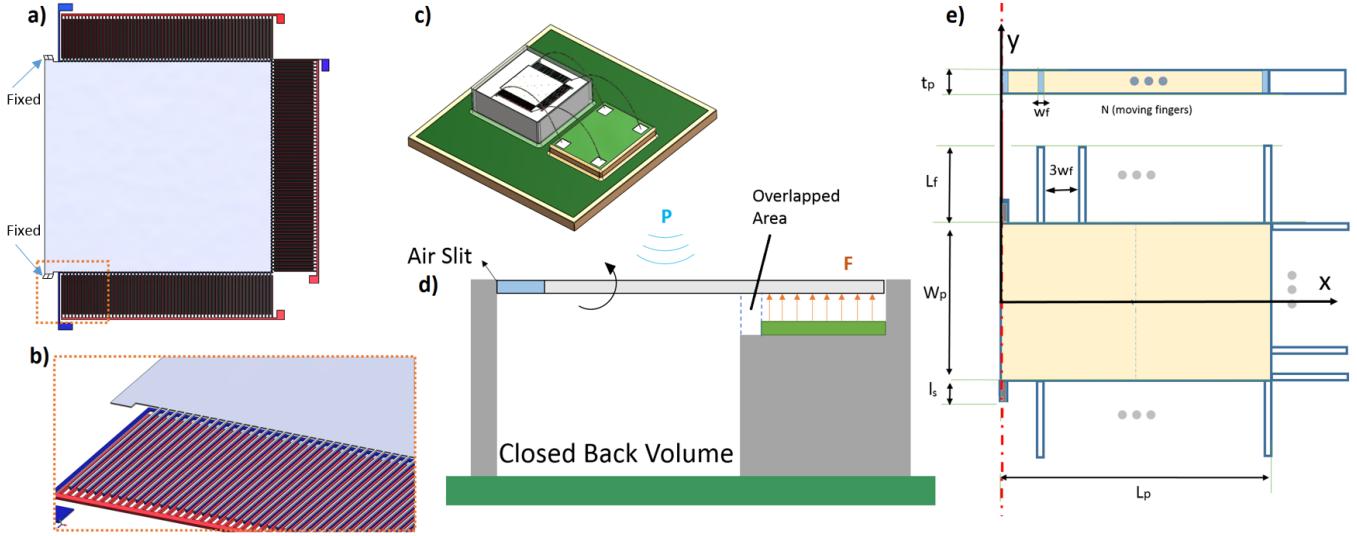
FIGURE 3: a) Schematic of a MEMS microphone with repulsive sensors b) A close-up of the fingers (Red fingers are voltage applied fixed fingers, blue fingers are grounded fixed fingers, gray fingers are grounded moving fingers) c) 3D Model with Circuit Board d) Cros-sectional view of the model with applied forces e) Design parameters are listed in Table 2 .

travel of the moving finger as plotted in Figure (5a). The corresponding repulsive force is obtained from $F = \frac{1}{2}\frac{dC}{dz}V^2$ as illustrated in Figure (5b). The simulated results are compared for the four different cases.

In order to predict the dynamic response of the system using Equation (3), capacitance must be written in a mathematical function, which is found from a polynomial fitting (7th order) on the finite element capacitance data of Figure (5a) when $w_f=4\,\mu m$, $t_f=4\,\mu m$ and $t_p=2\,\mu m$. The initial gap for three different widths (3, 4 and 5 μm) are chosen as 1.5 μm, 2 μm and 3 μm, respectively. These values are chosen for the diaphragm to oscillate about noting that the initial force obtained is repulsive (Figure (5b)). In this figure the repulsive force regimes also are shown for each case. The function for the capacitance per unit length is given in Equation (4) where a_0 through a_7 are the coefficients listed in Appendix A for all cases.

$$C_{unit}(z) = a_0 \cdot z^7 + a_1 \cdot z^6 + ... + a_6 \cdot z + a_7 \tag{4}$$

1 STATIC AND DYNAMIC SIMULATIONS

The static equilibrium position of the diaphragm can be found by assuming static pressure is negligible and setting the time functions to zero in Equation (3) which yields

$$K_t\theta = \frac{V^2}{2}\frac{dC}{d\theta} \tag{5}$$

Because the diaphragm has small rotations from the sound pressure, we can linearize the equation of motion using a Taylor expansion [27]. We assume ψ as a small rotation due to the sound pressure around the equilibrium rotation angle of θ_0. Then we substitute $\theta = \theta_0 + \psi$ in the Equation of Motion (6) and apply the Taylor series expansion. This yields to

$$I\ddot{\psi} + K_t(\theta_0 + \psi) + C_t\dot{\psi} = T + \frac{V^2}{2}\frac{dC}{d\theta}|(\theta_0 + \psi) \tag{6}$$

Taylor expansion of $\frac{dC}{d\theta}|(\theta_0 + \psi)$ can be expressed as

$$\frac{dC}{d\theta}|(\theta_0 + \psi) = \frac{dC}{d\theta}|(\theta_0) + (\psi)\frac{d^2C}{d\theta^2}|(\theta_0) \tag{7}$$

If we substitute Equation (7) in Equation (6), it yields

$$I\ddot{\psi} + C_t\dot{\psi} + \left(K_t - \frac{V^2}{2}\frac{d^2C}{d\theta^2}|(\theta_0)\right) \cdot \psi = T \tag{8}$$

where $K_t - \frac{V^2}{2}\frac{d^2C}{d\theta^2}|(\theta_0)$ can be redefined as K_{eff} which is the effective stiffness of the model. Depending upon the applied bias voltage and the second derivative of the capacitance with respect to the rotation angle, the frequency response of the diaphragm can shift to the left or right. For small rotations, the dynamic response can be assumed linear and one can find the the transfer function between the rotation angle ψ and the moment by the

5

FIGURE 4: Mechanical properties of the diaphragm are estimated using ANSYS. The modes and natural frequencies are shown. Mass of the diaphragm with fingers is 0.558×10^{-8} kg

sound wave, T:

$$H_{T\psi}(\omega) = \frac{1}{K_{eff} - I\omega^2 + j\omega C_t} \qquad (9)$$

where ω is the driving frequency. The harmonic sound wave pressure can be expressed as $P = \bar{P}e^{j(\omega t)}$. Here, $\bar{P}$ is the amplitude of the pressure, ω is the frequency of the sound wave. The applied moment from the sound pressure is written as $T(t) = PAL_p/2$ where P is function of pressure with respect to time, A is the surface area of the diaphragm and L_p is the length of the diaphragm. Using these equations, we can determine the transfer function between rotation angle and pressure as

$$H_{\bar{P}\psi}(\omega) = \frac{-AL_p/2}{K_{eff} - I\omega^2 + j\omega C_t} \qquad (10)$$

To obtain the electric voltage output, a charge amplifier circuit is used as in Figure (6). The advantage of using the charge amplifier is that the overall sensitivity is not affected by parasitic capacitance [15]. The amplifier has a direct effect on the sensitivity of the sensor so we have to find the electrical sensitivity by obtaining transfer function between output voltage and the rotation angle of the diaphragm.

$$H_{\psi V_0}(\omega) = -(1/C_f) \cdot V \frac{dC}{d\theta}|_{\theta_0} \qquad (11)$$

6
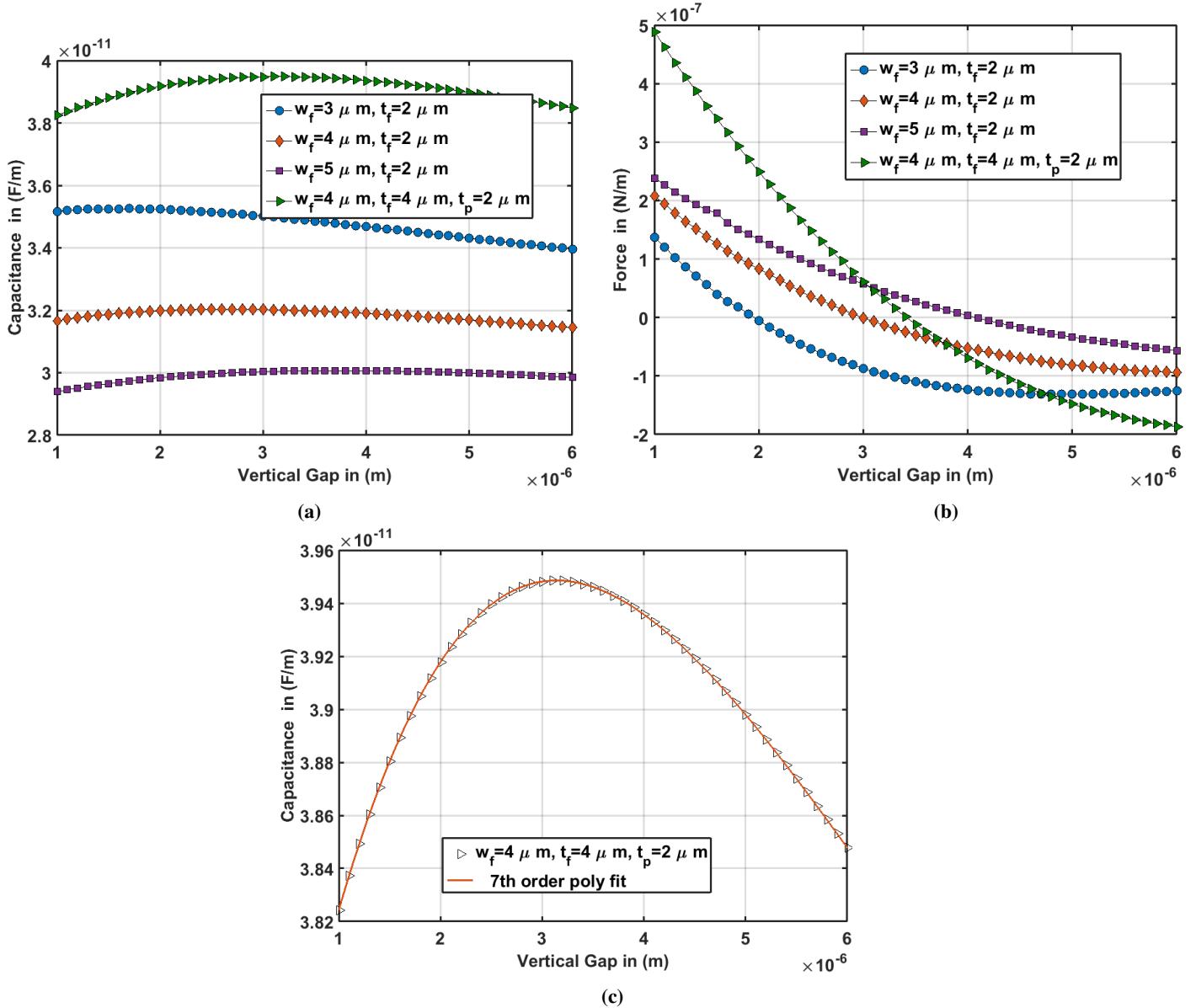
FIGURE 5: a)Capacitance simulations of different finger widths by FEA b) Repulsive force simulations of different finger widths by FEA a) Repulsive force simulation by COMSOl, b)Capacitance simulations of different finger widths by COMSOl

The electrical output (acoustic sensitivity) of the device may be determined by

$$H_{\bar{P}V_0}(\omega) = H_{\psi V_0} \times H_{\bar{P}\psi} \qquad (12)$$

Equation (12) gives the acoustic sensitivity of a rotating microphone. However, all of the air openings and the back volume of the microphone design have to be taken into consideration. In the next section we will present the related derivations to better understand the effect of back volume and air slits based on the study presented by Cui et al. [40].

Back Volume and Air Vent Effects

Back volume has an important effect on diaphragm response as it increases the effective stiffness and damping of the device. To investigate the effect of air openings in our model we assumed a piston-like translational motion as depicted in Figure (3). If a diaphragm is exposed to incident sound wave the response may

7

Description	Parameter	Value
Plate width	W_p	$990 \, \mu m$
Plate length	L_p	$1026 \, \mu m$
Plate thickness	t_p	$2 \, \mu m$
Moving finger length	L_f	$200 \, \mu m$
Moving finger thickness	t_p	$2 \, \mu m$
Voltage finger thickness	t_f	$2,4 \, \mu m$
Ground finger thickness	t_P	$2 \, \mu m$
Fixed finger width	w_f	$3,4,5 \, \mu m$
Initial gap	H	$2 \, \mu m$
Spring thickness	t_s	$2 \, \mu m$
Spring width	w_s	$40 \, \mu m$
Slit Length	w_{slit}	$1000 \, \mu m$
Slit Depth	h_{slit}	$2 \, \mu m$
Slit Width (half)	d_{slit}	$1 \, \mu m$
Air Density	ρ_0	$1.206 \, kg/m^3$
Air Viscosity	μ_{air}	$1.846 \times 10^{-5} \, kg/ms$
Sound Velocity	c	$344 \, m/s$
Young's Modulus	E	$170 \, GPa$
Polysilicon density	ρ	$2300 \, kg/m^3$
Air permittivity	ε_0	$8.854 \times 10^{-12} \, F/m$
Mass Moment of Inertia	I	$2.3361 \times 10^{-15} \, kgm^2$

TABLE 2: MEMS microphone dimensions presented in Figure 3
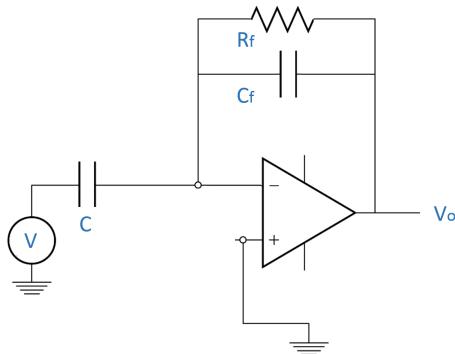
FIGURE 6: (Color online) Charge amplifier has Rf=10 $G\Omega$ and the capacitance Cf is 1pF [27].

be given as:

$$m\ddot{z} + kz + C\dot{z} = -PA \quad (13)$$

where m, k and C are the effective mass of the diaphragm, its mechanical stiffness and the damping coefficient, respectively. The mechanical stiffness and damping coefficients may be found as $k = 4\pi^2 f^2 m$ and $C = 2\zeta \sqrt{k \cdot m}$, respectively. In these equations

f is natural frequency and ζ is damping ratio. Our simulations are done by assuming ζ as 0.05. P is pressure from incoming sound wave and A is the surface area of the diaphragm. The volume in the back chamber will behave as a spring and increase the stiffness during the motion of the diaphragm. The pressure (P_d) resulted by the air molecules in the back volume exerts a force on the diaphragm and this force is balanced by a restoring force when the diaphragm moves out of plane.
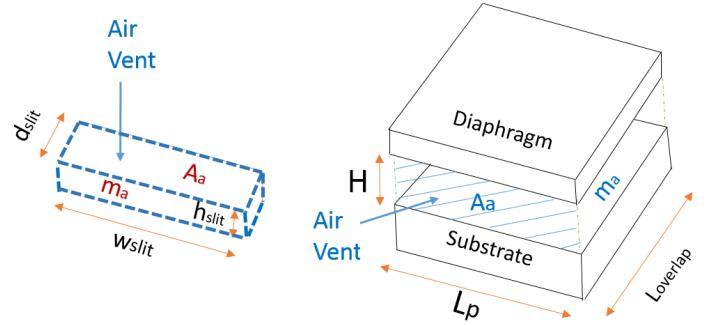
FIGURE 7: The figure shows the air vent areas such as slit and overlapped area.

The stiffness (K_d) of the fluctuating air molecules in the air chamber may be found as follows :

$$P_d = \rho_0 c^2 \frac{dV}{V} = -\rho_0 c^2 \frac{Ax}{V} \quad , \quad P_d A = -\rho_0 c^2 \frac{A^2 z}{V} = -K_d z \quad (14)$$

where ρ_0 is density of air, c is sound speed, V is back volume. From equation (14) stiffness can be found as $K_d = \rho_0 c^2 A^2 / V$ which effects mechanical stiffness and needs to be added to Equation (13). Hence, total mechanical stiffness becomes ($k + K_d$). In addition to back volume, slits (air vents around the diaphragm to release diaphragm from the substrate) also have an effect on the response of the microphone. The fluctuating air in the slit behaves like a moving mass (m_a) and causes coupling in the response of the diaphragm. With the same approximation in Equation (14), it can be given as

$$P_{aa} = -\rho_0 c^2 \frac{A_a z_a}{V} \quad , \quad P_{aa} A_a = -\rho_0 c^2 \frac{A_a^2 z_a}{V} = -K_{aa} z_a \quad (15)$$

where A_a is the area of the air slits and air openings under the diaphragm as seen in Figure (7). In our model $A_a = L_{slit} \times w_{slit} + H \times (2L_p + W_p)$. From Equation (15) stiffness from air openings can be found as $K_{aa} = \rho_0 c^2 A_a^2 / V$. The motion of this air mass

8

also exerts a force on the diaphragm. This force may be obtained as

$$P_{aa}A = -\rho_0 c^2 \frac{A_a A z_a}{V} = -K_{ad} z_a \quad (16)$$

where $K_{ad} = \rho_0 c^2 A_a A/V$. Also, the flapping of the diaphragm generates a force on the air mass. It can be written as

$$P_d A_a = -\rho_0 c^2 \frac{A_a A z}{V} = -K_{da} z \quad (17)$$

where $K_{da} = K_{da}$. Viscous effects in these air vents causes squeeze film damping. The restoring force from this air slit is presented by [40] as

$$F_{aa} = -C_v \cdot z$$
$$C_v = \frac{6\mu_{air} \times h_{slit} \times w_{slit}}{d_{slit}} + \frac{2\mu_{air} \times L_p^3 \times L_{overlap}}{H^3} + \frac{\mu_{air} W_p^3 \times L_{overlap}}{H^3} \quad (18)$$

where C_v is squeeze film damping coefficient, h_{slit} is the depth of the air in the slit, d_{slit} is the half of the width of the air slit, w_{slit} is the total length of the air slit. μ_{air} is air viscosity. $L_{overlap}$ is the length of the diaphragm that overlaps the substrate as seen in Figure (3). The overlap area behaves like a seal around the diaphragm and reduces the cut-off frequency. The chosen overlap length is 20 microns. Based on Figure (7), the surface area of the diaphragm and overlap area may be thought of as two parallel plates to simplify the damping calculations. Using this idea we estimated the damping in equation (18) which gives a rough estimation of the damping coefficient for initial calculations.

Applied external forces on the diaphragm and air slits due to incident sound wave are $F = -PA + F_{rep}$ and $F_a = -PA_a$. Hence, if we sum up all the forces we can find the response of the diaphragm by having a coupled equation as

$$m\ddot{z} + (k + K_d)z + (K_{ad})z_a + C\dot{z} = -PA + F_{rep}$$
$$m_a \ddot{z}_a + (K_{aa})z_a + (K_{da})z + C_v \dot{z}_a = -PA_a \quad (19)$$

where F_{rep} is the repulsive force generated on the fingers attached to diaphragm and may be given as $(V^2/2).dC/dz$. The effective stiffness is found in the same way described previously as $(k - \frac{V^2}{2} \cdot \frac{d^2C}{dz^2}|(z_0))$ and will be denoted as K_e for further calculations. The static equilibrium position of the diaphragm is solved by equation $K_e.z = V^2/2 dC/dz$.

The vertical displacement of the center of the moving fingers is depicted in Figure (8a) for different cases. The figure

shows that increasing the bias voltage results in a distinct response for each finger width. Moreover, we observed that the diaphragm will stay stationary beyond a certain voltage. Figure (8b) shows the normalized total capacitance versus applied bias voltage. Normalized values are obtained with respect to the maximum for each finger widths. Obtained maximum capacitance values are presented in the caption of the same figure. The largest slope is observed when width and thicknesses of the voltage applied fingers are 4 μm.

The response from the harmonic sound wave can be obtained by assuming $z = \bar{Z}e^{i\omega t}$ and $P = \bar{P}e^{i\omega t}$. Solving coupled equation gives the mechanical response (sensitivity) of the microphone. The transfer functions that predict the mechanical and acoustical sensitivities are found with the same method in Section (1).

$$H_{PZ}(\omega) = \frac{\bar{Z}}{\bar{P}} = \frac{A_a K_{ad} - A \times (K_{aa} + i\omega C_v - \omega^2 m_a)}{-K_{ad}K_{da} + (Ke + i\omega C - \omega^2 m) \times (K_{aa} + i\omega C_v - \omega^2 m_a)}$$
$$H_{ZV}(\omega) = -(1/C_f) \cdot V \frac{dC}{dz}|z_0$$
$$H_{PV}(\omega) = H_{Pz_0} \times H_{z_0 V}$$

$$(20)$$

where $Ke = (K + Kd - \frac{V^2}{2} \frac{d^2C}{dz^2}|(z_0))$. Equation (20) gives mechanical (H_{Pz_0}), electrical ($H_{z_0 V}$) and acoustical (H_{PV}) sensitivities, respectively. Figure (8c) presents the change in the capacitance as the bias voltage changes. Based on equations (20), the data given in Figure (8c) is important to estimate the sensitivity of the model, because higher slope of the capacitance indicates higher sensitivity. Hence, one can conclude that the microphone design that has the width and thicknesses of the voltage fixed fingers of 4 μm can achieve the highest sensitivity compared to other finger widths. For this case the response of the diaphragm is simulated in Figures (9a),(9b), (10a), and (10b).

Figure (9a) shows the mechanical sensitivity of the diaphragm for closed back volume. We observed that the electrical stiffness does not have a significant effect on the mechanical behavior for closed back volume. Figure (9b) shows the effect of back volume on mechanical sensitivity when electrical stiffness is not included. In this figure, the mechanical response of the diaphragm is simulated for different back volume scenarios. The thickness of a silicon wafer, which will be chosen in the fabrication process will be around 380 μm. However, effective back volume depth might be larger or smaller. Thus, many scenarios are considered. These results show that the stiffening effect of back volume reduces the sensitivity. One can improve the sensitivity by having larger back volume. In a previous study, Cui et al. [40] showed that it was possible to have larger back volume effect by drilling a hole in the ceramic substrate and package.
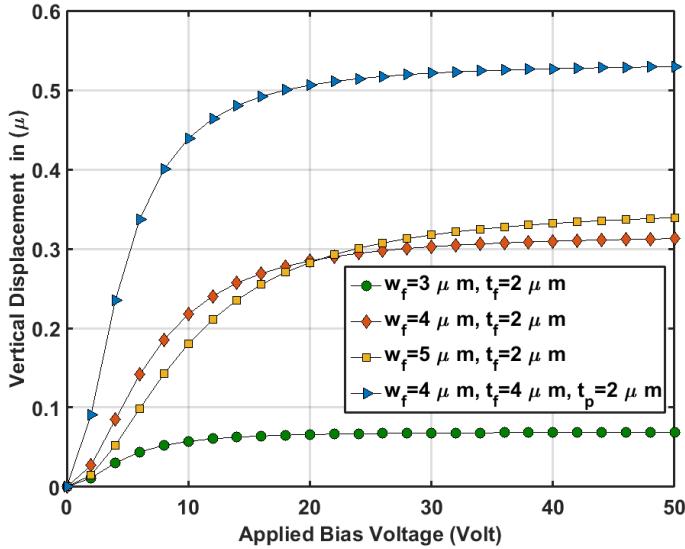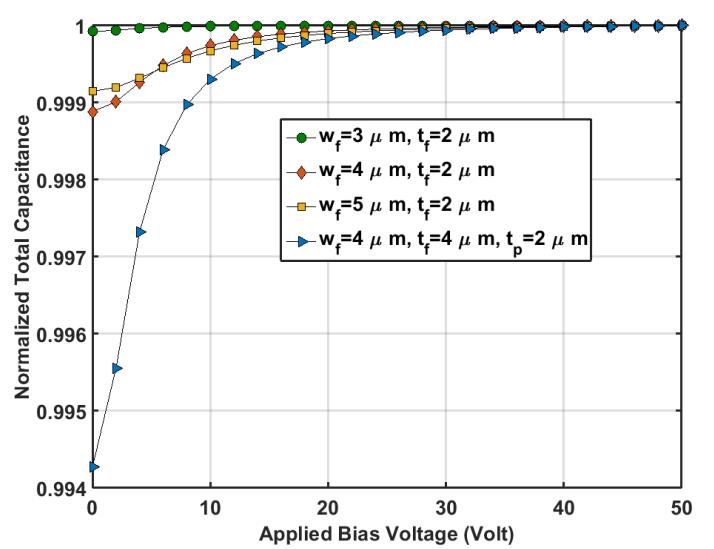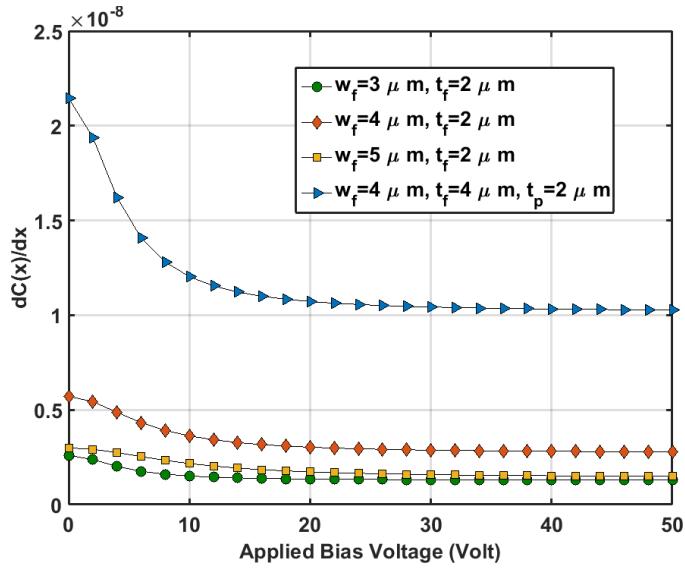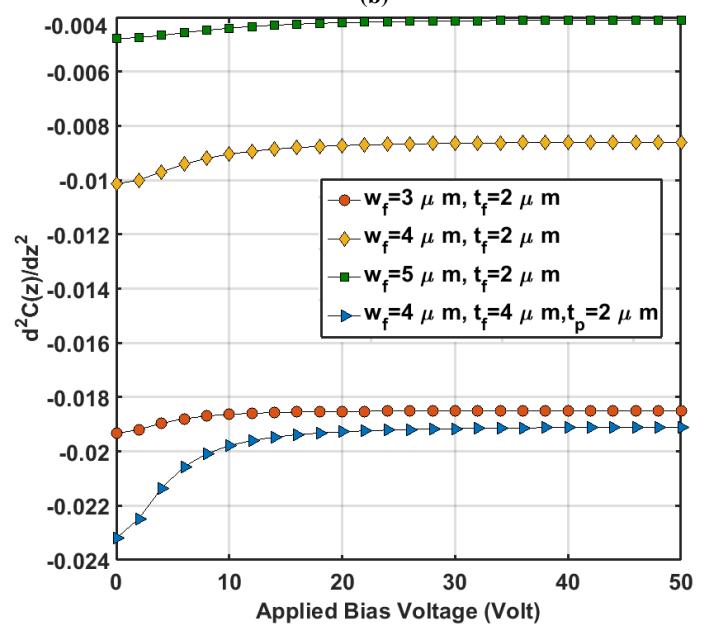
FIGURE 8: Different scenarios of finger width and thickness are simulated for a static situation: a) changes of the displacement of the finger with the bias voltage; b) total capacitance slope changes with the bias voltage. The obtained maximum capacitances are: (w_f=3 μm, t_f=2 μm), 1.7 pF. (w_f=4 μm, t_f=2 μm), 1.17 pF. (w_f=5 μm, t_f=2 μm), 0.8 pF and (w_f=4 μm , t_f=4 μm), 1.4 pF. c) The first derivative of the function of capacitance with respect to vertical displacement d) The second derivative of the function of the capacitance with respect to vertical displacement.

In Figure (10a) we observed that when the back volume is open, the sensitivity increases up to certain bias voltage. This happens due to the rapid growth of electrical stiffness with respect to second power of applied bias voltage. When the back side is closed we observed that the larger the bias voltage, the higher the acoustical sensitivity, as depicted in Figure (10b). Morever, we observed that the response of the diaphragm is very flat, which is a desired response in microphone design. It enables us to have a constant sensitivity at audible range of (20 Hz-20 kHz).

Copyright © 2016 by ASME
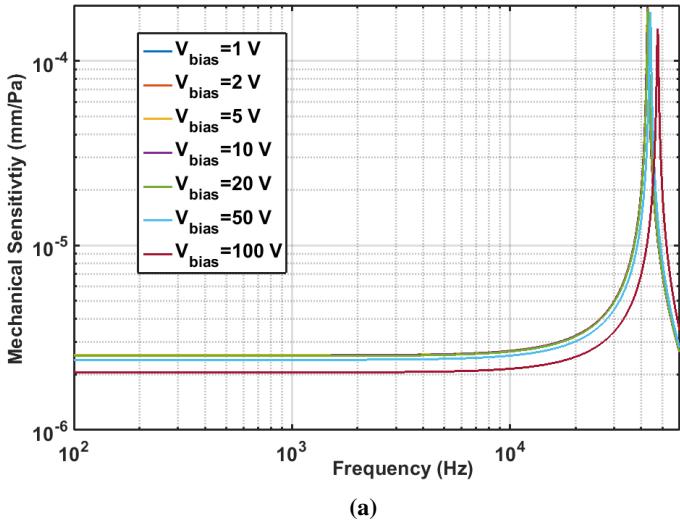
(a)
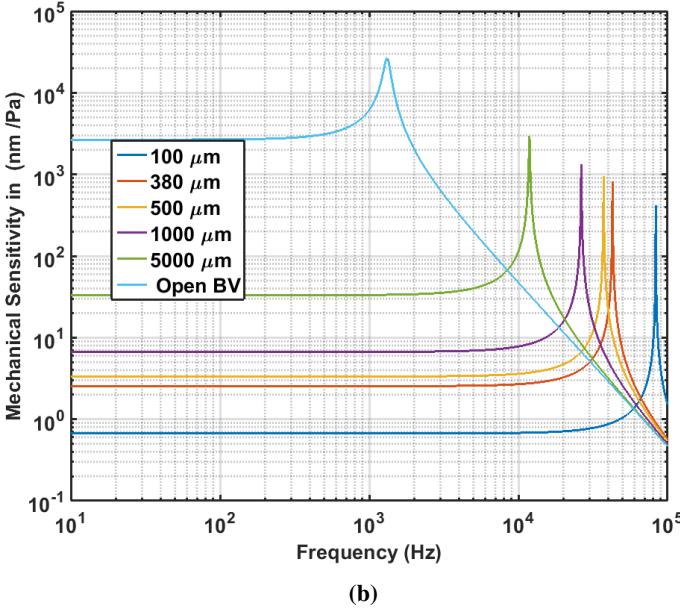
(b)

FIGURE 9: a) The mechanical sensitivity of the diaphragm for closed back volume ($380\mu m$). Damping ratio (ζ) is chosen as 0.05. b) Effect of the back volume for mechanical sensitivity when electrical stiffness effect is not included.

(a)

(b)

FIGURE 10: a) Acoustic sensitivity of the model when the back side is open. b) Acoustic Sensitivity for the case of closed back volume (Back volume depth is $380\ \mu m$).

CONCLUSION

In the present study, a microphone using the repulsive sensors is simulated. Because pull-in instability has been a significant and challenging design parameter for a MEMS device many

alternative methods have been presented to avoid it. Using the repulsive force is one technique that has been only used for MEMS actuators to date. In this study we employ the repulsive force concept for capacitive sensing in a MEMS microphone. Our simulations show that the sensitivity can be improved much more by increasing bias voltage without facing instabilities. In addition, the back volume has a significant effect on the sensitivity of the microphone that has been thoroughly investigated here. The estimated sensitivities are promising compared to the reported values in the literature. This study can be a pioneer work for future

11

applications of capacitive repulsive sensors.

REFERENCES

[1] Huang, P., Guo, J., Megerian, C., Young, D., and Ko, W., 2007. "A laboratory study on a capacitive displacement sensor as an implant microphone in totally implant cochlear hearing aid systems". In Engineering in Medicine and Biology Society, 2007. EMBS 2007. 29th Annual International Conference of the IEEE, pp. 5691–5694.

[2] Ko, W. H., Zhang, R., Huang, P., Guo, J., Ye, X., Young, D. J., and Megerian, C. A., 2009. "Studies of mems acoustic sensors as implantable microphones for totally implantable hearing-aid systems". *Biomedical Circuits and Systems, IEEE Transactions on, 3*(5), pp. 277–285.

[3] Tiete, J., Domínguez, F., Silva, B. d., Segers, L., Steenhaut, K., and Touhafi, A., 2014. "Soundcompass: a distributed mems microphone array-based sensor for sound source localization". *Sensors, 14*(2), pp. 1918–1949.

[4] Hougen, D. F., Benjaafar, S., Bonney, J. C., Budenske, J. R., Dvorak, M., Gini, M., French, H., Krantz, D. G., Li, P. Y., Malver, F., et al., 2000. "A miniature robotic system for reconnaissance and surveillance". In Robotics and Automation, 2000. Proceedings. ICRA'00. IEEE International Conference on, Vol. 1, IEEE, pp. 501–507.

[5] Zwyssig, E., Lincoln, M., and Renals, S., 2010. "A digital microphone array for distant speech recognition". In Acoustics Speech and Signal Processing (ICASSP), 2010 IEEE International Conference on, IEEE, pp. 5106–5109.

[6] Miles, R. N., and Hoy, R. R., 2006. "The development of a biologically-inspired directional microphone for hearing aids". *Audiol Neurotol, 11*(2), pp. 86–94.

[7] Mohamad, N., Iovenitti, P., and Vinay, T., 2007. "High sensitivity capacitive MEMS microphone with spring supported diaphragm". In Device and Process Technologies for Microelectronics, MEMS, Photonics, and Nanotechnology IV, Vol. 6800.

[8] Yang, C.-T., 2010. "The sensitivity analysis of a mems microphone with different membrane diameters". *Journal of Marine Science and Technology, 18*(6), pp. 790–796.

[9] Vahdat, A. S., Rezazadeh, G., and Afrang, S., 2011. "Improving response of a {MEMS} capacitive microphone filtering shock noise". *Microelectronics Journal, 42*(5), pp. 614 – 621.

[10] Wang, Z., Zou, Q., Song, Q., and Tao, J., 2015. "The era of silicon mems microphone and look beyond, microphone using coupled membrane structure". In Solid-State Sensors, Actuators and Microsystems (TRANSDUCERS), 2015 Transducers - 2015 18th International Conference on, pp. 375–378.

[11] Gharaei, H., Koohsorkhi, J., Saniei, F., and Abbasi, A., 2013. "Design and characterization of a high sensitive mems capacitive microphone using coupled membrane structure". In Robotics and Mechatronics (ICRoM), 2013 First RSI/ISM International Conference on, pp. 374–377.

[12] Fraden, J., 2004. *Handbook of modern sensors: physics, designs, and applications*. Springer Science & Business Media.

[13] He, S., and Mrad, R. B., 2005. "Large-stroke microelectrostatic actuators for vertical translation of micromirrors used in adaptive optics". *Industrial Electronics, IEEE Transactions on, 52*(4), pp. 974–983.

[14] Royer, M., Holmen, J., Wurm, M., Aadland, O., and Glenn, M., 1983. "Zno on si integrated acoustic sensor". *Sensors and Actuators, 4*, pp. 357–362.

[15] Martin, D. T., Liu, J., Kadirvel, K., Fox, R. M., Sheplak, M., and Nishida, T., 2007. "A micromachined dual-backplate capacitive microphone for aeroacoustic measurements". *Microelectromechanical Systems, Journal of, 16*(6), pp. 1289–1302.

[16] Williams, M. D., Griffin, B. A., Reagan, T. N., Underbrink, J. R., and Sheplak, M., 2012. "An aln mems piezoelectric microphone for aeroacoustic applications". *Microelectromechanical Systems, Journal of, 21*(2), pp. 270–283.

[17] Baumgartel, L., Vafanejad, A., Chen, S.-J., and Kim, E. S., 2013. "Resonance-enhanced piezoelectric microphone array for broadband or prefiltered acoustic sensing". *Microelectromechanical Systems, Journal of, 22*(1), pp. 107–114.

[18] Zhou, Z., Rufer, L., and Wong, M., 2014. "Damped aeroacoustic microphone with improved high-frequency characteristics". *Microelectromechanical Systems, Journal of, 23*(5), pp. 1094–1100.

[19] Bucaro, J. A., Lagakos, N., Houston, B. H., Jarzynski, J., and Zalalutdinov, M., 2005. "Miniature, high performance, low-cost fiber optic microphone". *The Journal of the Acoustical Society of America, 118*(3), pp. 1406–1413.

[20] Kuntzman, M. L., Garcia, C. T., Onaran, A. G., Avenson, B., Kirk, K. D., and Hall, N. A., 2011. "Performance and modeling of a fully packaged micromachined optical microphone". *Microelectromechanical Systems, Journal of, 20*(4), pp. 828–833.

[21] Hall, N. A., and Degertekin, F. L., 2002. "Integrated optical interferometric detection method for micromachined capacitive acoustic transducers". *Applied Physics Letters, 80*(20), pp. 3859–3861.

[22] Miles, R. N., Su, Q., Cui, W., Shetye, M., Degertekin, F. L.,

Bicen, B., Garcia, C., Jones, S., and Hall, N., 2009. "A low-noise differential microphone inspired by the ears of the parasitoid fly ormia ochracea". *The Journal of the Acoustical Society of America,* **125**(4), pp. 2013–2026.

[23] Rombach, P., Müllenborn, M., Klein, U., and Rasmussen, K., 2002. "The first low voltage, low noise differential silicon microphone, technology development and measurement results". *Sensors and Actuators A: Physical,* **95**(2), pp. 196–201.

[24] Martin, T., Kadirvel, K., Fox, R., Nishider, T., Liu, J., and Sheplak, M., 2005. "Surface and bulk micromachined dual back-plate condenser microphone". In Micro Electro Mechanical Systems, 2005. MEMS 2005. 18th IEEE International Conference on, IEEE, pp. 319–322.

[25] Hohm, D., and GerhardMulthaupt, R., 1984. "Silicondioxide electret transducer". *The Journal of the Acoustical Society of America,* **75**(4), pp. 1297–1298.

[26] Bergqvist, J., and Gobet, J., 1994. "Capacitive microphone with a surface micromachined backplate using electroplating technology". *Microelectromechanical Systems, Journal of,* **3**(2), pp. 69–75.

[27] Miles, R., Cui, W., Su, Q., and Homentcovschi, D., 2015. "A mems low-noise sound pressure gradient microphone with capacitive sensing". *Microelectromechanical Systems, Journal of,* **24**(1), Feb, pp. 241–248.

[28] Marques, A. F., Castelló, R. C., and Shkel, A., 2005. "Modelling the electrostatic actuation of mems: state of the art 2005". *Reports de recerca de l'Institut d'Organització i Control de Sistemes Industrials*(18), p. 1.

[29] Younis, M. I., 2011. *MEMS linear and nonlinear statics and dynamics*, Vol. 20. Springer Science & Business Media.

[30] Lee, K. B., 2007. "Non-contact electrostatic microactuator using slit structures: theory and a preliminary test". *Journal of Micromechanics and Microengineering,* **17**(11), p. 2186.

[31] Krylov, S., Ilic, B. R., and Lulinsky, S., 2011. "Bistability of curved microbeams actuated by fringing electrostatic fields". *Nonlinear Dynamics,* **66**(3), pp. 403–426.

[32] Linzon, Y., Ilic, B., Lulinsky, S., and Krylov, S., 2013. "Efficient parametric excitation of silicon-on-insulator microcantilever beams by fringing electrostatic fields". *Journal of Applied Physics,* **113**(16), p. 163508.

[33] Ouakad, H. M., 2015. "Numerical model for the calculation of the electrostatic force in non-parallel electrodes for mems applications". *Journal of Electrostatics,* **76**, pp. 254–261.

[34] Lee, K. B., and Cho, Y.-H., 2001. "Laterally driven electrostatic repulsive-force microactuators using asymmetric field distribution". *Microelectromechanical Systems, Journal of,* **10**(1), pp. 128–136.

[35] He, S., and Ben Mrad, R., 2008. "Design, modeling, and demonstration of a mems repulsive-force out-of-plane electrostatic micro actuator". *Microelectromechanical Systems, Journal of,* **17**(3), June, pp. 532–547.

[36] He, S., Ben Mrad, R., and Chang, J., 2010. "Development of a high-performance microelectrostatic repulsive-force rotation actuator". *Microelectromechanical Systems, Journal of,* **19**(3), June, pp. 561–569.

[37] Hu, F., Yao, J., Qiu, C., and Ren, H., 2010. "A mems micromirror driven by electrostatic force". *Journal of Electrostatics,* **68**(3), pp. 237–242.

[38] Towfighian, S., He, S., and Mrad, R. B., 2014. "A low voltage electrostatic micro actuator for large out-of-plane displacement". In ASME 2014 International Design Engineering Technical Conferences and Computers and Information in Engineering Conference, American Society of Mechanical Engineers, pp. V004T09A015–V004T09A015.

[39] Zhou, J. Miles, R., and Towfighian, S., 2015. "A novel capacitive sensing principle for microdevices". In ASME 2015 International Design Engineering Technical Conferences and Computers and Information in Engineering Conference, pp. 659–662.

[40] Cui, W., Miles, R. N., and Su, Q., 2009. "A robust miniature silicon microphone diaphragm". *Sensors & Transducers,* **7**, p. 63.

Appendix A: Coefficients of Fitting Functions For Case 1-4

Coef.	$w_f = 3\mu m$, $t_f = 2\mu m$	$w_f = 4\mu m$, $t_f = 2\mu m$	$w_f = 5\mu$
a_0	-2.06944×10^{25}	6.34629×10^{24}	-1.184
a_1	4.96528×10^{20}	-1.55445×10^{20}	3.4589
a_2	-4.63875×10^{15}	1.70078×10^{15}	-4.091
a_3	18586147662.6525	-12193537772.8112	2446610
a_4	4543.76321	74788.07996	-6610
a_5	-0.344914360777564	-0.39688	-0.0
a_6	9.02172×10^{-7}	$1.12633649949011 \times 10^{-6}$	8.3378
a_7	3.45951×10^{-11}	3.08713×10^{-11}	2.86699

TABLE 3: Coefficients of fitted functions for different finger widths and thickness.